Optical, physical, and chemical properties of tar balls observed during the Yosemite Aerosol Characterization Study

J. L. Hand,[1] W. C. Malm,[2] A. Laskin,[3] D. Day,[1] T. Lee,[4] C. Wang,[3] C. Carrico,[4] J. Carrillo,[4] J. P. Cowin,[5] J. Collett Jr.,[4] and M. J. Iedema[3]

Received 21 December 2004; revised 16 May 2005; accepted 23 August 2005; published 9 November 2005.

[1] The Yosemite Aerosol Characterization Study of summer 2002 (YACS) occurred during an active fire season in the western United States and provided an opportunity to investigate many unresolved issues related to the radiative effects of biomass burning aerosols. Single particle analysis was performed on field-collected aerosol samples using an array of electron microscopy techniques. Amorphous carbon spheres, or "tar balls," were present in samples collected during episodes of high particle light scattering coefficients that occurred during the peak of a smoke/haze event. The highest concentrations of light-absorbing carbon from a dual-wavelength aethalometer (λ = 370 and 880 nm) occurred during periods when the particles were predominantly tar balls, indicating they do absorb light in the UV and near-IR range of the solar spectrum. Closure experiments of mass concentrations and light scattering coefficients during periods dominated by tar balls did not require any distinct assumptions of organic carbon molecular weight correction factors, density, or refractive index compared to periods dominated by other types of organic carbon aerosols. Measurements of the hygroscopic behavior of tar balls using an environmental SEM indicate that tar balls do not exhibit deliquescence but do uptake some water at high ($\sim$83%) relative humidity. The ability of tar balls to efficiently scatter and absorb light and to absorb water has important implications for their role in regional haze and climate forcing.

Citation: Hand, J. L., et al. (2005), Optical, physical, and chemical properties of tar balls observed during the Yosemite Aerosol Characterization Study, *J. Geophys. Res.*, *110*, D21210, doi:10.1029/2004JD005728.

1. Introduction

[2] Carbonaceous aerosol emissions from biomass burning contribute significantly to the atmospheric aerosol burden on a global scale [*Bond et al.*, 2004]. Understanding the global climate effects and regional haze effects of carbonaceous aerosols requires an understanding of many complex issues related to primary and secondary production of these aerosols, including their composition, mixing properties, hygroscopicity, and resulting radiative properties. Distinguishing different carbonaceous particle types with electron microscopy provides useful information about aerosols emitted from biomass burning, where particle size, composition and the mixing state of carbonaceous aerosols can vary on the basis of formation processes, condensation of primary and secondary gases, and transport [e.g., *Osán et al.*, 2002; *Ebert et al.*, 2002; *Li et al.*, 2003a; *Pósfai et al.*, 2003, 2004]. In particular, a distinct carbonaceous particle type, called "tar balls" has been observed in plumes from southern African fires [*Li et al.*, 2003a; *Pósfai et al.*, 2003, 2004] and during other biomass burning events [*Cofer et al.*, 1988; *Gaudichet et al.*, 1995; *Martins et al.*, 1996, 1998; *Alfaro et al.*, 2003]. *Pósfai et al.* [2004] report that tar balls are amorphous carbon balls, distinct from soot, and probably correspond to an intermediate stage in the aging of organic particles from biomass burning. They also propose a gas-to-particle formation mechanism that suggests tar balls are high–molecular weight organic polymer species that are believed to be water-insoluble and may be slightly absorbing in the visible spectrum range.

[3] The purpose of this study is to further investigate the optical and hygroscopic properties of tar balls by examining contemporaneous aerosol measurements during periods when tar balls were the dominant aerosol type. An extensive suite of measurements was performed during a field campaign at Yosemite National Park to characterize the physicochemical, optical, and hygroscopic properties of biomass smoke aerosols. The Yosemite Aerosol Char-

[1]Cooperative Institute for Research in the Atmosphere, Colorado State University, Fort Collins, Colorado, USA.
[2]National Park Service, Cooperative Institute for Research in the Atmosphere, Colorado State University, Fort Collins, Colorado, USA.
[3]William R. Wiley Environmental Molecular Sciences Laboratory, Pacific Northwest National Laboratory, Richland, Washington, USA.
[4]Department of Atmospheric Science, Colorado State University, Fort Collins, Colorado, USA.
[5]Chemical Sciences Division, Pacific Northwest National Laboratory, Richland, Washington, USA.

0148-0227/05/2004JD005728$09.00

acterization Study (YACS) was conducted from July to September of 2002 [*Malm et al.*, 2005a; *Carrico et al.*, 2005; *McMeeking et al.*, 2005a]. The campaign occurred during an active fire season in the western United States. Major forest fires in southern Oregon burned hundreds of thousands of acres during the study. Back trajectory analyses suggest flow patterns consistent with long-range transport of smoke to the study site during periods when the site was engulfed by regional smoke and haze [*McMeeking et al.*, 2005a].

[4] Aerosol $PM_{2.5}$ mass concentrations increased during one such haze episode that occurred around mid-August (day of year, DOY, 228–230) (see first panel of Figure 1). Particulate organic matter (POM), determined using thermal optical reflectance (TOR) [*Chow et al.*, 1993], dominated the fine mode aerosol composition during the study (69% of fine mass on average), especially during the haze episode of mid-August when fractional contributions exceeded 80% of the fine mass (see second panel of Figure 1 and *Malm et al.* [2005a] for details about the measurements). Large diurnal variations in carbonaceous aerosols were observed, as shown by the POM data derived from the Rupprecht and Patashnick (R and P) model 5400 Ambient Carbon Particulate Monitor [*Rupprecht et al.*, 1995]. Elemental carbon (EC) concentrations from 24-hour samples analyzed with the TOR method are shown in third panel of Figure 1. Black carbon (BC) concentrations (15-min samples) from a dual-channel AE21 McGee Scientific aethalometer are plotted with EC and demonstrate diurnal variations and elevated levels during the smoke/haze episode. Inorganic species contributed less to fine mass than carbonaceous aerosols on average [*Lee et al.*, 2003], but played a larger role at the beginning and end of the study (especially sulfate, see fourth and fifth panels in Figure 1).

[5] The effect on visibility from the increase in aerosol loading during the smoke/haze event is evident in the elevated $PM_{2.5}$ aerosol light scattering coefficients (b_{sp}) measured with nephelometry (see sixth panel of Figure 1) [*Day and Malm*, 2003; *Malm et al.*, 2005b]. It was estimated that POM contributed over 90% to b_{sp} during the haze episode, and 84% on average [*Malm et al.*, 2005a]. Variations in the aerosol size distribution were also observed during periods of elevated levels of b_{sp}, with aerosol size distributions shifting to larger size and also narrowing [*McMeeking et al.*, 2005a]. These changes in the aerosol physical properties may be due to aging [*McMeeking et al.*, 2005a], or to changes in the particle morphology. The YACS study provided an excellent opportunity to investigate the individual particle morphology and mixing characteristics of biomass smoke aerosols in relation to their ensemble average optical, chemical, and physical properties. We specifically investigate these relationships for tar balls and report for the first time some estimates of their ensemble average physical and optical properties and single particle hygroscopic properties.

[6] This paper is organized in five sections. The experimental method is described in section 2. Results from analyses of individual particles are presented in section 3. Section 4 presents comparisons of single particle data with other measurements, and implications for visibility and climate studies. A summary of the results is provided in section 5.

2. Experimental Method

[7] Yosemite National Park is located in the central Sierra Nevada in California. The sampling site was located at Turtleback Dome at the IMPROVE site (Interagency Monitoring of Protected Visual Environments [*Malm et al.*, 1994]) on the south rim of the entrance to Yosemite Valley (119.7 W, 37.71 N, 1615 meters). The Time Resolved Aerosol Collector (TRAC) sampler [*Laskin et al.*, 2003, 2005a] was used to collect aerosol samples for computer-controlled scanning electron microscopy with energy-dispersed detection of X rays (CCSEM/EDX) for individual particles. The TRAC was deployed for almost four weeks of sampling (10 August to 5 September 2002) during which 15-min samples were collected. The TRAC is a conventional one stage jet-to-plate impactor. The aerosols were deposited on a rotating impaction plate with prearranged thin film TEM grid substrates. Carbon Type-B (Ted Pella, Inc., Redding, California) 50-nm thick films supported by 400-mesh copper mesh grids were used. Each substrate was exposed individually to the impactor nozzle for a preset time. The effective cutoff size (D_{50}) of the impactor is $\sim$0.36 μm.

[8] CCSEM/EDX analysis of the aerosol samples was performed using a FEI XL 30 digital field emission gun scanning electron microscope. X rays from elements with an atomic number higher than beryllium ($Z > 4$) were detected by an EDAX PV7761/54 ME spectrometer with a Si(Li) detector of an active area of 30 mm^2 and ATW2 window. The system is equipped with Genesis® hardware and software (EDAX, Inc) for CCSEM/EDX particle analysis. Fields of view were set over the sample area and automatically inspected on a field-by-field basis. In each field of view, particles are recognized by an increase of the detector signal above a preselected threshold level, using a mixed signal of backscattered and transmitted electrons [*Laskin et al.*, 2005b]. Particles with equivalent circle diameters larger than 0.08 μm were detected by the software, and X-ray spectra were acquired from each detected particle larger than 0.2 μm. The X-ray spectra were acquired for 10 seconds of clock time, at a beam current of 400–500 pA and an accelerating voltage of 20 kV. We used a magnification of $\times$4000. About 1500–2000 individual particles per sample were probed by CCSEM/EDX, resulting in $\sim$48,000 analyzed particles.

[9] The EDX composition data were quantified by means of a method that relates the measured X-ray intensity to an elemental concentration using calculated equivalent X-ray intensities of corresponding elements. Specific details of the Genesis® microanalysis method can be found elsewhere [*Hua*, 2003]. We omitted corrections related to atomic number–dependent electron scattering (Z), absorption (A), and fluorescence (F), because ZAF effects are generally considered minimal for micron- and submicron-size particles mounted on thin film substrates [*Armstrong*, 1991]. The elements detected in particles for this work were C, N, O, Na, Si, S, Cl, and K. The atomic percent data for the light elements such as C, O and N are regarded as semiquantitative, considering C and O contributions from the thin film

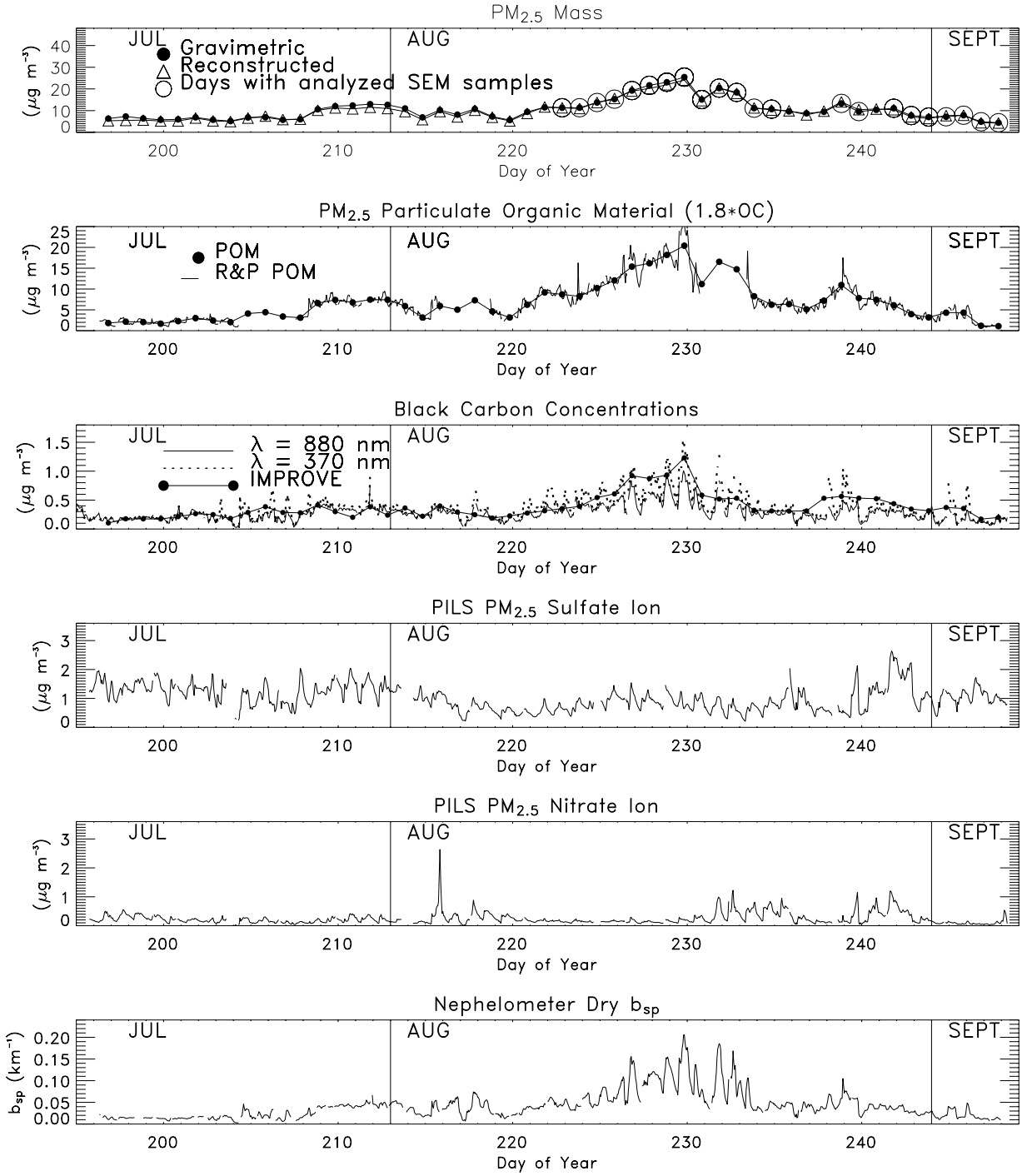

Figure 1. Timeline of $PM_{2.5}$ bulk aerosol composition ($\mu g\ m^{-3}$) from PILS, IMPROVE, R and P, the dual-wavelength aethalometer (λ = 370 nm and 880 nm), and $PM_{2.5}$ dry b_{sp} (km^{-1}) measured with a nephelometer.

substrate, and the transmission characteristics of the ATW2 window that overlaps with the K_α line of nitrogen. The effects of beam damage and beam-induced chemical reactions in particles may additionally modify particle composition. Nevertheless, the method has been proven instrumental for distinguishing particle morphology and mixing properties, and for studying the temporal evolution of particle composition [e.g., *Laskin and Cowin*, 2001; *Osán et al.*, 2002; *Ebert et al.*, 2002; *Laskin et al.*, 2002, 2003, 2005a, 2005b; *Li et al.*, 2003a, 2003b; *Pósfai et al.*, 2003, 2004; *Godoi et al.*, 2004].

[10] Transmission Electron Microscopy (TEM) was performed to study the internal structure and composition of individual particles using a JEOL 2010 high-resolution (HR) TEM fitted with a LaB_6 filament and operated at 200 kV accelerating voltage. The TEM is equipped with an Oxford energy dispersive X-ray (EDX) spectrometer with ISIS analysis software (Oxford, Inc.), enabling identifica-

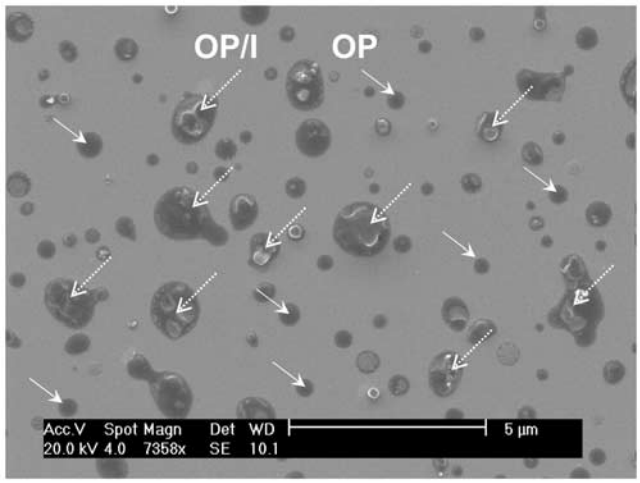

Figure 2. Organic particles with (OP/I) and without inclusions (OP) (sample DOY 228.73). Particles with no inclusions are shown with solid arrows, and particles with inclusions are shown with dashed arrows.

tion of elements with atomic number higher than beryllium ($Z > 4$). The TEM is also equipped with a Gatan Image Filter (GIF), allowing for elemental maps of particles at high spatial resolution to be obtained through electron energy loss spectrometry (EELS) and corresponding energy filtered imaging based on EELS.

[11] Hygroscopic properties of tar balls were investigated using the FEI XL30 SEM operated in the environmental mode (ESEM), which allows for imaging with up to ~15 Torr of water vapor present in the chamber [*Danilatos*, 1993]. The temperature of the specimen was maintained at 5°C using a Peltier stage. The water vapor pressure within the chamber was increased from 2.9 to 6.5 Torr (45–100% relative humidity, RH) and morphological changes were recorded using computer video recorder software. The imaging conditions of the ESEM require a balance between a strong beam that can focus through water vapor (high energy and high current) and minimizing damage to particles (low energy and low current). An accelerating voltage of 15 keV, beam current of 150 pA, and fast scanning conditions (linetime 1.68 ms, 1452 lines per frame) were found optimal in previous hydration studies using the same instrument [*Hoffman et al.*, 2004], and were applied in the hydration studies presented here.

3. Results From SEM Analyses

3.1. Particle Types Identified From YACS

[12] Prominent types of biomass smoke particles were distinguished by means of electron microscopy, similar to previous studies [e.g., *Osán et al.*, 2002; *Ebert et al.*, 2002; *Li et al.*, 2003a, 2003b; *Pósfai et al.*, 2003, 2004]. The open circles in the first panel of Figure 1 indicate sample periods analyzed with electron microscopy. The characteristics used to distinguish particles were particle morphology, internal structure, volatility and susceptibility to damage by the electron beam. Automated classification of particle types from CCSEM/EDX data is difficult for biomass smoke particles because morphology signatures (an important feature of biomass smoke particles) are not always readily discernible from composition, size or shape information available from the CCSEM/EDX data. For example, "round" particles as defined by automated analysis of shape could be related to flat volatile films or spherical particles, and both might have similar sizes or compositions. Therefore, in order to quantify particle morphology, visual inspection of SEM images was performed. Several secondary electron images were acquired on different areas of a given sample, and these images were visually inspected to assess and assign particles to four major types: tar balls, semivolatile organic particles with (or without) inclusions, nonvolatile particles, and soot. These types are defined and described below. The average number of total particles inspected per sample was ~200, and 59 samples were inspected. The frequency of occurrence of a particle type was determined by counting the number of particles of a given type and dividing it by the total number of all particles counted in inspected images. At least one 15-min sample per day was inspected from DOY 222–248 (with the exception of DOY 236 and 240), but not always at the same time each day, and most days had several 15-min sample inspected. Therefore the frequency of the inspected samples is not continuous.

[13] The most abundant particle type observed corresponded to organic particles with or without inclusions (OP/I). They accounted for 47% of visually inspected particles from YACS, with frequencies ranging from 0 to 99% for a given sample. Roughly 46% of OP/I particles did not have inclusions (or 22% of the visually inspected particles). An example SEM image of this type of particle is shown in Figure 2. At 20 kV imaging, organic constituents of particles are largely electron-transparent and therefore are seen as dark areas that may or may not surround a bright inclusion. These dark areas were subject to damage from the electron beam. The organic nature of these particles is inferred from the SEM/EDX analysis of particles having no bright inclusions. Their EDX spectra show no elements other than C, O and probably N. EDX inspection of the bright inclusions indicates the presence of K, S, Cl, Si, and Na, similar to the data reported by *Pósfai et al.* [2003, 2004] for organic particles with inclusions. The particle morphology suggests that these particles were probably hydrated during sampling and spread against the substrate at the time of impaction. They may have also substantially dehydrated in the vacuum chamber of the SEM, and most likely lost volatile species.

[14] The second most abundant particle type observed was tar balls (TB). Tar balls accounted for 30% of visually inspected samples, ranging from 0 to 94%. Tar balls are readily recognized in SEM and TEM images by their spherical shape and amorphous carbon morphology (Figure 3). HRTEM images of tar balls at high magnification do not indicate any semiordered graphitic microstructure typical of soot. Their EDX and EELS spectra indicate elemental compositions consisting of C and O and probably N, with trace amounts of S, K, Cl, Si and Na. Internal mixing of tar balls with other particle types was rarely observed. Tar balls do not volatilize under vacuum of SEM or TEM, nor do they change visibly when exposed to the electron beam. TEM images and EELS maps of the tar balls (Figures 3 and 4) reveal their internal structure that includes

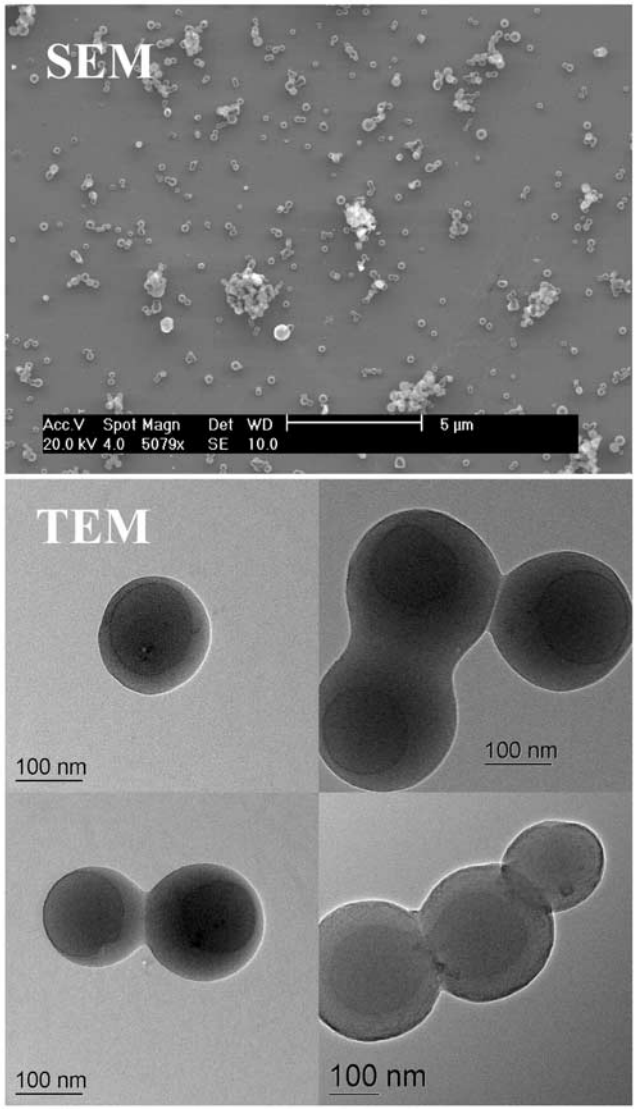

Figure 3. Tar ball (TB) SEM and TEM images (sample DOY 229.853). Tar balls are shown as individual spherical particles, as well as in agglomerates.

a spherical core and an outer shell. Homogeneous internal distributions of C and O in tar balls were previously reported by *Pósfai et al.* [2003, 2004]. However, electron energy loss maps shown in Figure 4 indicate that while the distributions of C and possibly N in the tar balls from YACS are fairly homogeneous, the concentration of O is strongly enhanced in the ~30 nm outer layer of the particle. *Maria et al.* [2004] speculate that atmospheric processing of organic carbon particles could result in larger concentrations of carbonyl carbon (oxygenated hydrocarbons) at the surface of the particle for small particles with large surface-area-to-volume ratios (surface-limited reactions).

[15] These tar ball properties are generally consistent with what has been previously reported, however, there are characteristics that clearly distinguish the tar balls observed in this study from those reported previously [*Pósfai et al.*, 2003, 2004]. The tar balls observed during YACS are larger in size compared to those found in the smoke from Mozambique and Brazil biomass fires [*Martins et al.*, 1998; *Pósfai et al.*, 2003, 2004], and in the samples from the K-puszta site (Hungary) where the tar balls were associated with local household wood combustion [*Pósfai et al.*, 2004] (see discussion in section 3.2). Figure 3 clearly indicates agglomeration of tar balls in clusters that also was not typical for some of the previous studies. In the YACS samples, small clusters of a few tar balls were very common and larger clusters consisting of tens of individual tar balls were also evident. As will be shown below, the tar balls sampled during YACS were aged two or more days during transport to the sampling site, while the tar balls reported by *Pósfai et al.* [2003, 2004] were sampled from young (a few hours old) biomass smoke. Therefore perhaps prolonged atmospheric processing of tar balls could explain the observed differences between the tar balls observed during YACS and those properties described by *Pósfai et al.* [2003, 2004].

[16] The third most abundant particle type observed was nonvolatile particles (NV), accounting for 23% of all inspected particles (ranging from 0 to 97%). These particles had no dark areas corresponding to organic constituents and are seen in the SEM as bright features of irregular shape. They are not beam sensitive and do not evaporate under prolonged exposure to the electron beam, as indicated by

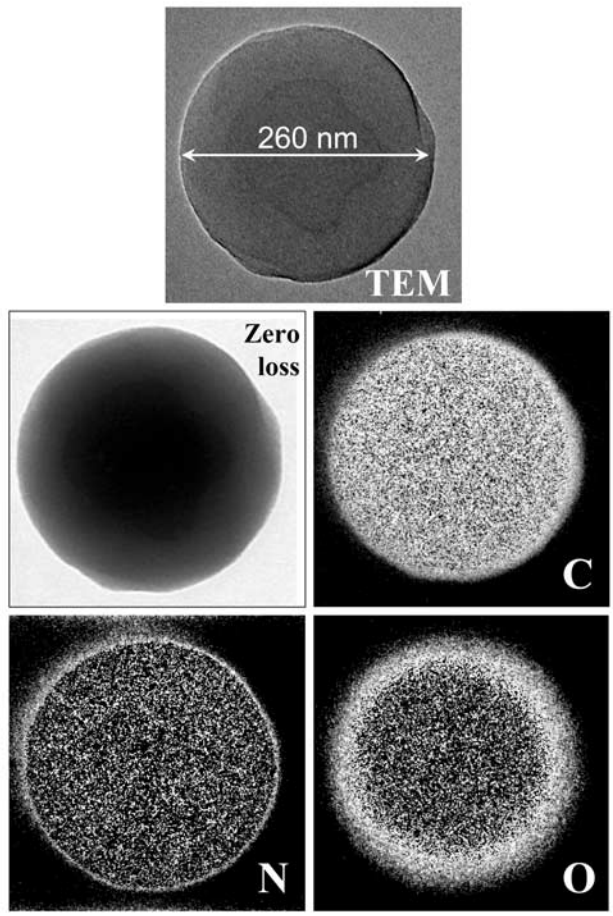

Figure 4. TEM image and EELS maps of a tar ball particle from a bright-field zero loss map, carbon map, nitrogen map, and oxygen map (sample DOY 229.853).

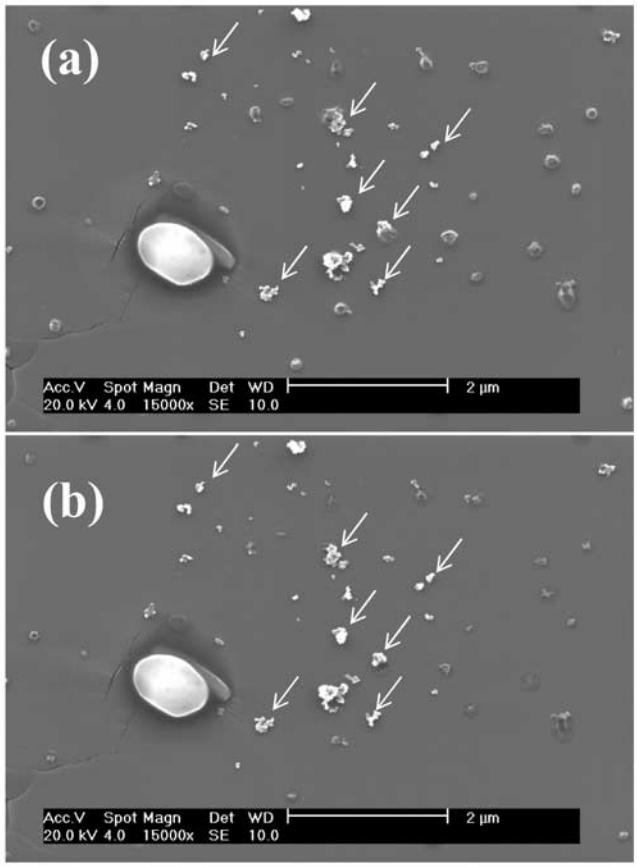

Figure 5. Bright nonvolatile (NV) particles are shown (a) before and (b) after CCSEM/EDX analysis (sample DOY 237.51). Arrows point to some of the NV particles.

two SEM images taken before and after CCSEM/EDX analysis (see Figures 5a and 5b). The particles that are affected by exposure in the right section of Figures 5a and 5b are of the OP/I particle type. In addition to C and O, EDX analyses show variable concentrations of K, Cl, S, Si, Na and Ca in the NV particles. Other common inorganic particles, such as fly ash, sea salt (i.e., the micron-size particle in the SEM images of Figures 5a and 5b), and some typical mineral dust constituents were also detected, although infrequently.

[17] The least abundant particle type observed was soot. Soot particles are distinguishable by their unique morphology. They consist of chain aggregates of individual spherules 20–50 nm in size [e.g., *Ishiguro et al.*, 1997; *Pósfai et al.*, 2003, 2004]. These spherules are composed of concentric curved graphite layers similar to the layers of an onion (see SEM, TEM and HRTEM images in Figure 6). Soot particles accounted for only 0.3% of visually inspected particles (ranging from 0 to 5%). However, it is possible that aged, collapsed soot could be present as inclusions of organic particles, as hinted at by the appearance of some particles in Figure 6. Collapsed aged soot particles were also observed by *Zuberi et al.* [2005] as part of laboratory studies.

[18] The frequency of occurrence of particle types varied during the study. A semicontinuous timeline of the major particles types is shown in Figure 7. The OP/I type particles were dominant from DOY 222 to mid-228, DOY 229, and toward the end of the study, when the NV type particles were also present (consistent with higher concentrations of bulk inorganic aerosol concentrations during that period, see Figure 1). Tar balls were dominant on most samples from DOY 228.5–233.5 with the highest frequency of their occurrence (above ~80%) for many samples between DOY 229 and DOY 233. Both tar ball and OP/I type particles were dominant during periods with high POM concentrations (POM > 10 $\mu g\ m^{-3}$).

3.2. Description of Particles From CCSEM/EDX

[19] The carbon background signal from the TEM grid makes it difficult to quantify the absolute carbon concentration of particles. No correction of the background is possible because it varies from particle to particle, as does the actual particle carbon signal. However, semiquantitative CCSEM/EDX data are fairly consistent with the bulk composition data. The CCSEM/EDX analysis suggests high atomic percents of carbon in most of the particles analyzed during YACS, in fact, C + O > 95% for 68% of the ~48,000 particles analyzed with CCSEM/EDX. Carbon atomic percents were less than 70% in only 0.7% of particles. Sulfur was detected in only 43% of the particles, K in 5% of the particles, Si in 21%, Na in 3%, and Cl was detected in 0.7% of particles (see Table 1 for a summary). Less than 1% of the particles were probably "pure" ammoniated sulfate (S+O+N+C = 100%). Sulfur tended to be mixed with Si (11% of all particles had S-Si) rather than with potassium

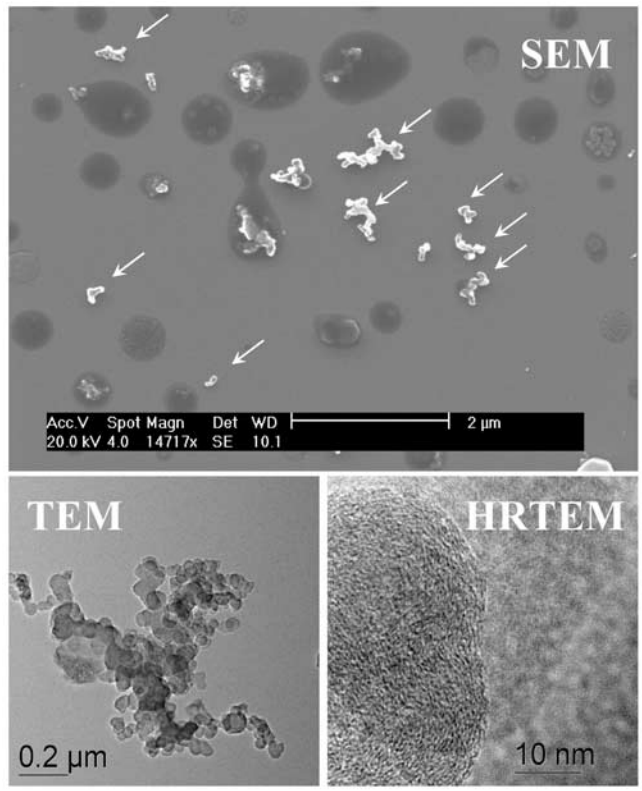

Figure 6. Typical soot particles from SEM, TEM and HRTEM images (sample DOY 228.729). Arrows point to soot particles.

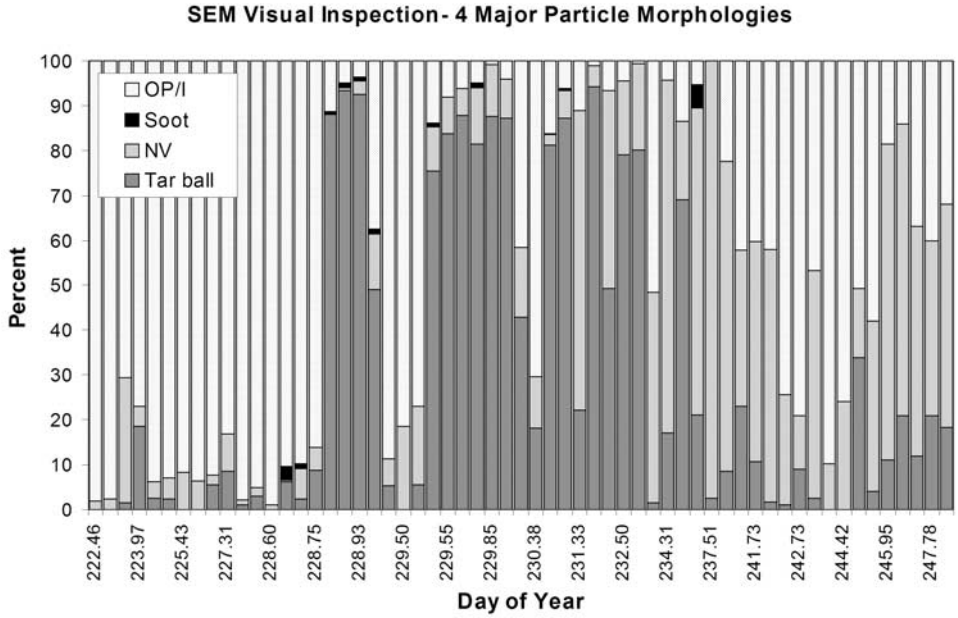

Figure 7. Frequency of occurrence (as percent, %) of four particle types: tar balls, organic with (and without) inclusions (OP/I), nonvolatile particles (NV), and soot.

(2% had S-K) (Table 2). Other elements associated with inorganic compounds were more likely to be mixed with sulfur than not (see Tables 2 and 3). With the exception of silicon, combinations of K, Na, and Cl occurred for less than 1% of nonsulfur bearing particles (see Table 3). Inorganic particles analyzed during YACS were usually internally mixed to some degree.

[20] Ternary diagrams are useful for understanding the mixing characteristics of particles [e.g., *Li et al.*, 2003a; *Pósfai et al.*, 2003; *Yuan et al.*, 2004]. Data that congregate at an apex of the triangle are composed of higher fractions of that element compared to the other two elements represented. Data within the triangle represent particles that are internal mixtures of at least three represented elements. The mixing characteristics of tar balls and the OP/I particles are generally consistent with what has been previously reported [*Pósfai et al.*, 2003, 2004]. Both particles types contain carbon, oxygen, and trace amounts of S, K, Si, Na and Cl. Ternary diagrams shown in Figure 8 demonstrate that the mixing characteristics between these particle types are not easily distinguishable. For example, sample DOY 225.426 is dominated by the OP/I type (92%). Its ternary diagram of C-O-(Na+K+S+Cl+Si) indicates the presence of elements other than C and O, although C and O are dominant. Tar balls may have less additional elements, for example, sample DOY 229.853 is dominated by tar balls (88%), and the data congregate near the carbon apex (Figure 8). However, not all tar balls exhibit similar mixing properties. For example, sample DOY 228.835 is dominated by tar balls (93%), and indicates more substantial contributions from noncarbon elements compared to sample DOY 229.853.

[21] The elemental ratios of inorganic elements in smoke-influenced aerosols can be indicative of the aging or degree of atmospheric processing of the particles [*Pósfai et al.*, 2003; *Li et al.*, 2003a]. Some of the differences observed between tar balls collected during YACS compared to other studies may be due to the degree of processing or aging of these particles. Young smoke particles have been observed to contain unprocessed KCl salt, while in aged smoke particles K_2SO_4 salt was evident [*Li et al.*, 2003a]. Ternary diagrams of Cl-K-S for samples dominated by tar balls (samples DOY 228.835 and DOY 229.853) indicate that some Cl was detected, however the detection of sulfur is indicative of processed smoke (Figure 9). These data are similar to far downwind fires observed by *Li et al.* [2003a] in southern African fires.

[22] Elemental ratios of S, O, and K also indicate that tar balls at YACS were aged smoke processed with sulfur (K_2SO_4). For example, in Figure 10, the tar ball samples (samples DOY 228.835 and DOY 229.853) show young smoke designated on the K-O axis and the addition of sulfur

Table 1. Summary of Mixing Characteristics of All Particles (~48,000) From 39 Samples in Terms of Percent of Total Particles[a]

Elements	S	No S	K	Si	Na	Cl	C < 70%	C > 95%	Na+Cl	C+O+N = 100%	C+O > 95%
Total, %	43	57	5	21	3	0.7	0.7	13	0.3	1.5	68
Maximum, %	88	93	10	73	9	3	3	63	2	9	96
Minimum, %	7	12	1.2	0.8	0.18	0	0	0.9	0	0	27

[a]The entry refers to the percent of total particles that has detectable limits of given element. The maximum (minimum) refers to the highest (lowest) percentage observed for a given sample.

Table 2. Summary of Mixing Characteristics of Particles Containing Sulfur (~21,000) From 39 Samples in Terms of Percent of Particles[a]

Elements	S-K	S-Si	S-Na	S-Cl	S-K-Si	S-Na-Cl	S-Na-K	S-K-Cl	S+C+O+N = 100%
Total, %	1.8	11	0.7	0.05	1.2	0.3	0.8	0.3	0.9
Maximum, %	5	53	3	.06	7	1.8	3	1.7	10
Minimum, %	0.09	0.09	0	0	0	0	0	0	0

[a]The entries refer to the percent of particles that have sulfur and other species mixed. The maximum (minimum) corresponds to the highest (lowest) percentage observed for a given sample.

that may occur with age. In addition, the EELS map in Figure 4 showed enhanced oxygen on the outer edge of the tar ball, which might be indicative of an aged particle that underwent oxidation reactions on its surface. Back trajectory calculations showed that air masses from the Oregon fires often traveled along the California coast, across the Bay area before reaching the site [*McMeeking et al.*, 2005a]. These particles were undergoing mixing processes in the atmosphere for 2–3 days before reaching the park, so the presence of processed, aged smoke aerosols is not unexpected.

[23] Particle size distributions can also be indicative of aging, as suggested by *McMeeking* [2004] from changes observed in the size distributions during YACS. Single particle diameter is determined by the SEM analysis software by computing the area-equivalent diameter of a circle from the measured pixel area converted to square micrometers. Recall that the minimum particle diameter characterized by the analysis software is 0.08 μm, and that the D_{50} of the TRAC sampler is around 0.36 μm, so collection efficiencies of small particles (~0.1 μm) are only a few percent [*Laskin et al.*, 2003]. The particles sampled during YACS were predominantly in the fine particle mode, with 92% of the particles having area-equivalent diameters less than 0.7 μm.

[24] Different particle types revealed different size characteristics. Size distributions were constructed for each sample by binning particles into a given size range based on their equivalent diameter, however, possible spreading due to impaction of the OP/I particles on the substrate makes analyzing size distributions from SEM difficult. Size distributions of tar balls are not affected by these issues because of their refractory and nonvolatile nature. Examples of tar ball number distributions from YACS are shown in Figure 11, along with the data for tar balls collected from southern Africa biomass smoke and from the K-puszta sampling site in Hungary [*Pósfai et al.*, 2004]. The collectors employed in our study and those of *Pósfai et al.* [2004] have similar cutoff characteristics ($D_{50} \sim 0.36$ μm and $D_{50} \sim 0.30$ μm, respectively); therefore the size distributions shown in Figure 11 are likely affected by poor collection efficiencies of small particles. However, these effects are less important for the particles larger than 0.3 μm [*Pósfai et al.*, 2003]. The tar balls observed in Yosemite National Park are significantly larger ($D_p \sim 0.3$ μm) than those collected in southern Africa ($D_p \sim 0.15$ μm) and K-puszta site ($D_p \sim 0.1$ μm). The size characteristics of tar balls observed during YACS have important implications for their ability to efficiently scatter light, as will be discussed in section 4.

3.3. Environmental SEM Analysis of Tar Ball Hygroscopic Properties

[25] *Pósfai et al.* [2004] have assumed that the organic polymer material of tar balls is mostly insoluble in water and therefore their sizes are not altered by the effects of relative humidity or by cloud processing. We employ the ESEM technique to investigate the hygroscopic behavior of tar balls. Images of tar balls corresponding to different values of relative humidity are shown in Figure 12. The first two images (taken at 60.0% and 73.3% RH, respectively) indicate no visible changes in particle morphology. The initial changes in particle morphology are observed at an RH of 83.4%. At this point, initial restructuring of some of the tar balls is evident by the blurring and "melting" of particle edges. Further increases in RH led to complete destruction of tar balls with the effective "melting" of their constituents as they dissolve. Two images taken at 92.0% and 99.0% RH demonstrate the degradation of the tar balls and wetting of the substrate by their dissolved constituents. The last image shows the same area of the substrate at 45% RH after completion of a full hydration/dehydration cycle. The image indicates full, irreversible destruction of the particles and formation of large spots on the substrate resulting from drying of the tar ball liquid. We note that the irreversibility of the morphology changes could be affected by the substrate and therefore is not necessarily the case for airborne tar balls.

4. Tar Ball Properties and Implications for Visibility Estimates and Climate Studies

[26] In this section we speculate on the chemical, optical, and hygroscopic properties of tar balls by investigating concurrent aerosol measurements and results derived from

Table 3. Summary of Mixing Characteristics of Particles Not Containing Sulfur (~27,000) From 39 Samples in Terms of Percent of Particles[a]

Elements	K	Si	Na	Cl	K-Si	Na-Cl	Na-K	K-Cl
Total, %	1.3	8	0.08	0	0.3	0.02	0.06	0.03
Maximum, %	4	49	0.6	0	1.6	0.3	0.4	0.3
Minimum, %	0.15	0.4	0	0	0	0	0	0

[a]The entries refer to the percent of particles containing elements other than sulfur. The maximum (minimum) refers to the highest (lowest) percentage observed for a given sample.

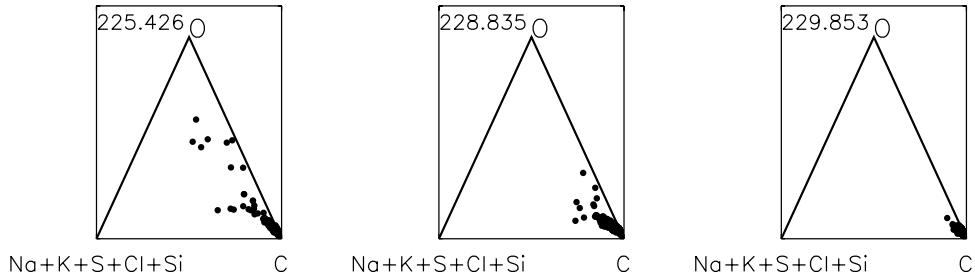

Figure 8. Ternary diagram of C-O-(Na+K+S+Cl+Si) for three samples (DOY 225.426, DOY 228.835, and DOY 229.853). The leftmost sample is dominated by OP/I particles (92%), while the other two samples are dominated by tar balls (93% and 88%, respectively).

closure studies during periods when tar balls were the dominant particle type. Most of these properties are derived from measurements that occurred with the same time resolution as the SEM samples and therefore can be used to estimate ensemble average tar ball properties. We discuss the role of tar balls in visibility estimates and climate studies on the basis of their properties reported here.

[27] The chemical composition and molecular speciation of tar balls has not yet been reported in the literature. *Pósfai et al.* [2004] speculated a gas-to-particle formation mechanism that suggests tar balls are a high–molecular weight polymer humic-like substance (HULIS) that is formed by OH radical induced polymerization of lignin constituents (e.g., guaiacol, syringol and their substituted derivatives) [*Mayol-Bracero et al.*, 2002; *Gelencsér et al.*, 2003; *Hoffer et al.*, 2004] that are typical products of wood pyrolysis [*Rogge et al.*, 1998]. Organic molecular weight to carbon weight (M_{Wt}/C_{Wt}) factors in the range of 1.5–1.9 can be computed from molecular formulas of lignin constituents reported for wood combustion [*Rogge et al.*, 1998]. Similar factors ranging from 1.9–2.1 were reported for particulate organic emissions from fireplace wood combustion of pine, oak and eucalyptus [*Turpin and Lim*, 2001]. On the basis of the biomass smoke origins of tar balls, it is realistic to assume that they have M_{Wt}/C_{Wt} factors falling within the range of 1.5–2.1. This assumption is consistent with the M_{Wt}/C_{Wt} factor of 1.8 used during YACS to achieve closure in 24-hour gravimetric and reconstructed mass concentrations shown in Figure 1 (first panel) [*Malm et al.*, 2005a]. However, this factor was applied for the entire study, even when tar balls were not the dominant particle type, suggesting other types of carbonaceous aerosols may have similar M_{Wt}/C_{Wt} ratios, especially when averaged over a 24-hour sample period.

[28] We saw no evidence of volatilization or electron beam damage of tar balls in the SEM, suggesting they are composed of refractory material. Furthermore, only minor amounts of soot particles were seen on the SEM samples, so EC as characterized by the TOR method was not soot. Others have reported that elemental carbon and a significant fraction of organic carbon from biomass smoke have similar volatility and combustion temperatures, causing the split between EC and OC to be poorly defined (and method-dependent) and leading to an overestimation of EC and an underestimation of OC for biomass smoke [*Novakov and Corrigan*, 1995; *Gelencsér et al.*, 2000; *Mayol-Bracero et al.*, 2002; *Guyon et al.*, 2003; *Formenti et al.*, 2003]. These previous studies and the ensemble average tar ball properties reported here suggest that the data from TOR analyses of biomass smoke should not be interpreted as an external mixture of organic and elemental carbon, but rather interpreted as nongraphitic carbonaceous particles that contains light absorbing molecules. The interpretation of EC and OC data as internally mixed in the calculation of ensemble tar balls optical properties is examined below.

[29] Measurements of light scattering coefficients (b_{sp}) suggest that tar balls are very efficient at light scattering. The highest values of b_{sp} (see Figure 1, sixth panel) occurred during periods when tar balls accounted for over 80% of the particle type. Reconstructed b_{sp} values were computed with Mie theory using size distribution data and volume-weighted refractive indices [*Ouimette and Flagan*, 1982; *Hasan and Dzubay*, 1983; *Malm et al.*, 2005a]. This method assumes an internally mixed aerosol, and the properties of each species in that internal mixture are weighted by their volume fraction. Complex refractive indices ($n = m + ki$) estimated from this method are sensitive to the assumed aerosol composition and the

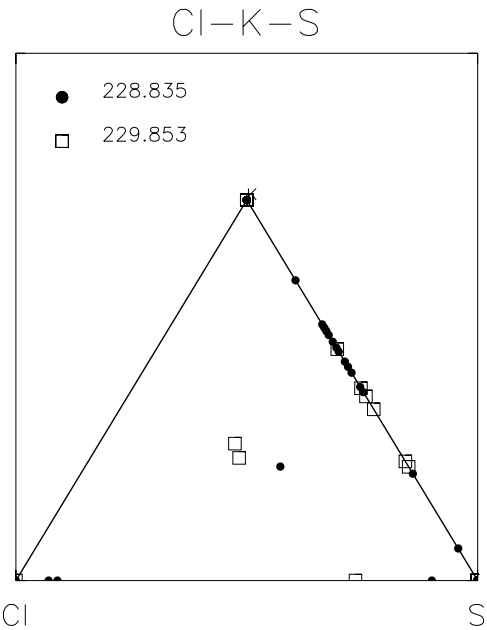

Figure 9. Ternary diagram of Cl-K-S for two samples dominated by tar balls (DOY 228.835 and DOY 229.853).

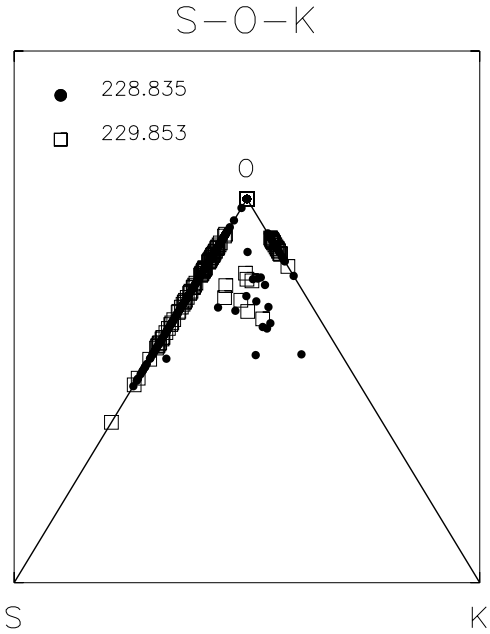

Figure 10. Ternary diagram of S-O-K for two samples dominated by tar balls (DOY 228.835 and DOY 229.853).

species' optical and physical properties; during YACS the method was especially sensitive to properties of organic carbon as it dominated the fine mass [*McMeeking et al.*, 2005b]. Although tar balls are amorphous refractory carbon and not soot, we considered EC and OC as separate constituents (as defined by TOR) and assigned properties specific to each. Typical values of OC refractive index and density (ρ) were assumed ($m = 1.55$ and $\rho = 1.4$ g cm^{-3}), and soot properties were applied to the aethalometer data normalized to the EC data from TOR ($n = 1.8 + 0.5i$, $\rho = 1.8$ g cm^{-3} [*Malm et al.*, 2005a]). Applying these OC and EC refractive indices to all time periods (regardless of particle morphology) in the calculation of reconstructed b_{sp} resulted in excellent agreement between measured and reconstructed b_{sp} within 4% on average. This agreement indicates that tar balls do not require unique assumptions of refractive index or density to obtain closure in b_{sp}.

[30] Mass scattering efficiencies (α_{sp}) that were computed from size distribution and composition data using the method just discussed [*Malm et al.*, 2005a] yielded estimates near 6 m^2 g^{-1} during time periods when tar balls were the predominant particle type (over 80%). It is evident that it was the size distribution characteristics of tar balls that were responsible for the high mass scattering efficiencies and not unique refractive indices, because the size distributions shifted to larger sizes and also narrowed during this time [*McMeeking et al.*, 2005a]. The high values of α_{sp} ($\sim$6 m^2 g^{-1}) are larger than values typically assumed for organic carbon aerosols ($\sim$4 m^{2}g^{-1} [*Malm et al.*, 1994]). Values of α_{sp} closer to 4 m^2 g^{-1} were estimated at the beginning and end of the study, although the same OC and EC properties (refractive index and density) were applied throughout.

[31] The derived ensemble average complex refractive indices of tar balls ($n = 1.56 + 0.02i$) imply that they do absorb light. Moreover, the absence of soot on the SEM samples and BC/OC ratios that were fairly constant throughout the study period suggest that not only tar balls but other types of nongraphitic carbonaceous particles were also responsible for light absorption. The ability of tar balls to absorb light across the visible and UV spectral range has been suggested from previous results of UV-VIS spectroscopy experiments of HULIS formed from lignin type precursors in model cloud water [*Mukai and Ambe*, 1986; *Gelencsér et al.*, 2003; *Hoffer et al.*, 2004] and is also supported by field measurements of absorption characteristics of forest fire particulates [*Patterson and McMahon*, 1984; *Foot and Kilsby*, 1989; *Bergstrom et al.*, 2002; *Guyon et al.*, 2003; *Kirchstetter et al.*, 2004].

[32] Further inspection of the aethalometer data provides qualitative information on the wavelength dependence of absorption of tar balls. The data from the dual wavelength aethalometer used during YACS are corrected for the λ^{-1}

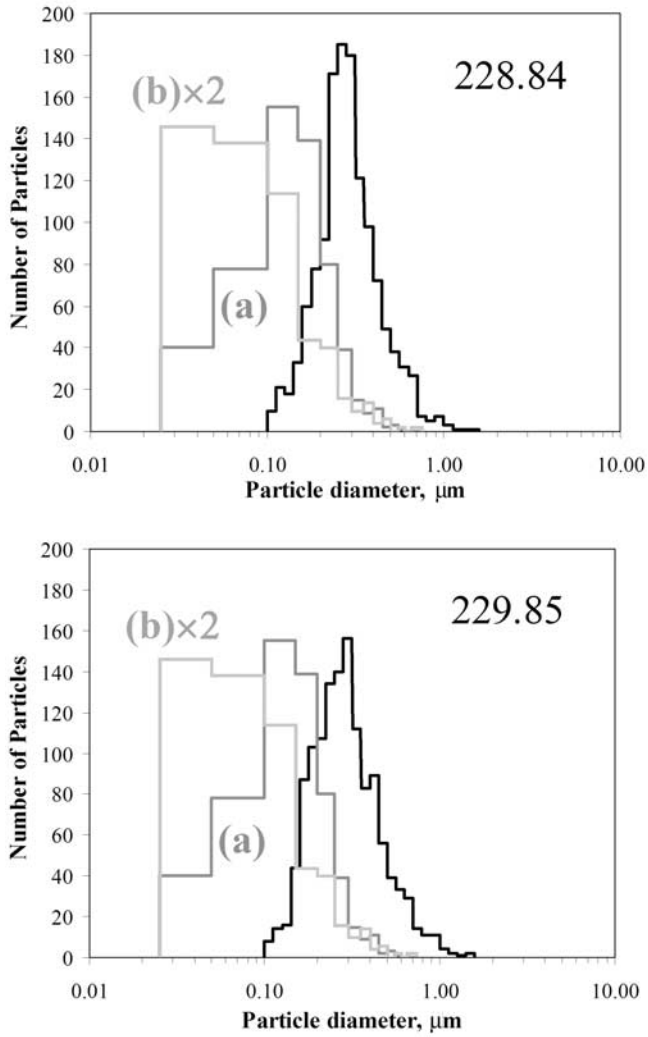

Figure 11. Tar ball number distributions from two YACS samples (DOY 228.84 and DOY 229.85) plotted along with tar ball size distributions reported for (a) southern Africa biomass smoke and (b) K-puszta site in Hungary [*Pósfai et al.*, 2004].

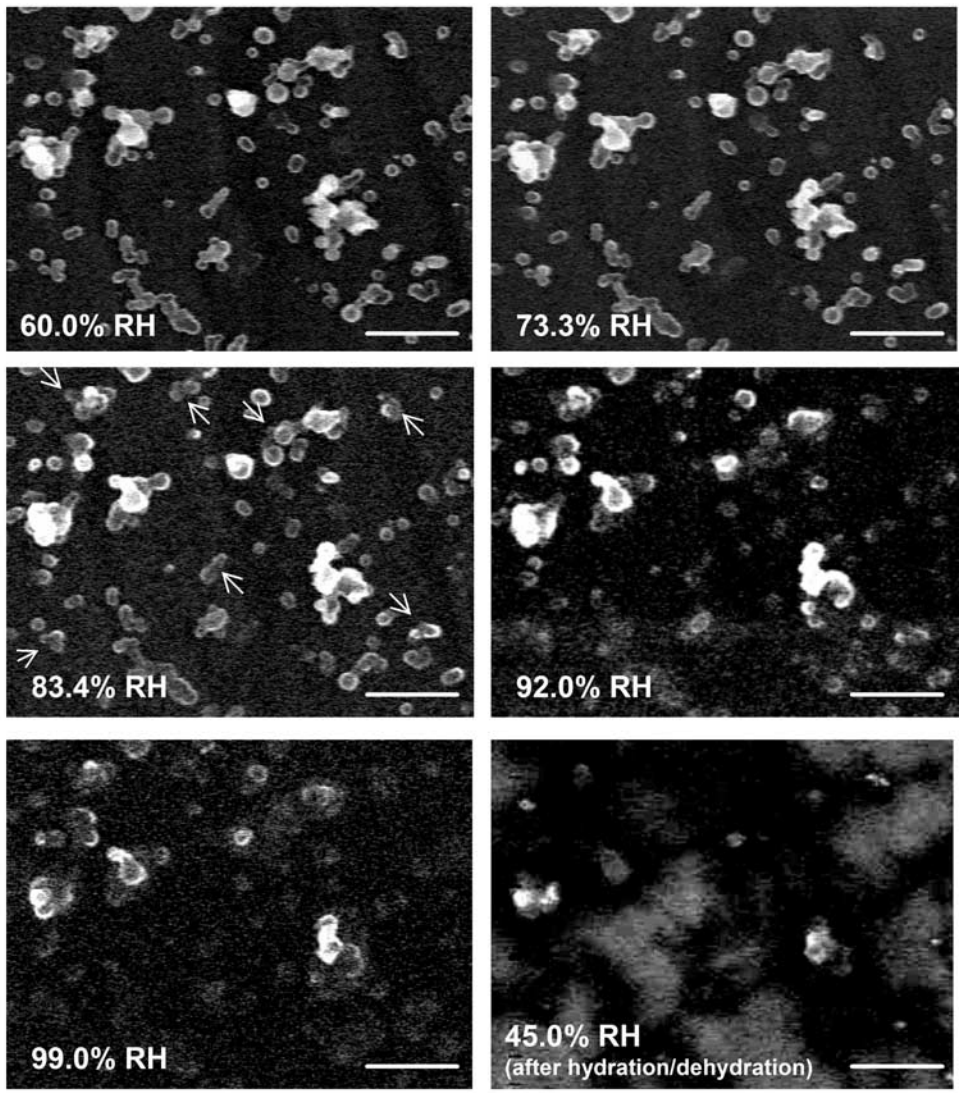

Figure 12. ESEM images of tar ball particles exposed to increasing relative humidity and then after completion of a hydration/dehydration cycle. Size bars on the micrographs depict 2 μm scale.

dependence of aerosol absorption by small particles [*Bohren and Huffman*, 1983], therefore any divergence between the concentrations from the two channels indicates the presence of absorbing (e.g., aromatic) species found in wood smoke [*Allen et al.*, 2004; *Kirchstetter et al.*, 2004]. Deriving quantifiable mass concentrations (or absorption coefficients) from the UV channel of the aethalometer is problematic because a linear relationship between mass and absorption may not apply for particles with sizes similar to the wavelength of the measurement [*Allen et al.*, 2004; T. Hansen, personal communication, 2004]. Therefore we report the difference in the BC concentrations from the UV and nIR channels as a qualitative indication of spectral absorption.

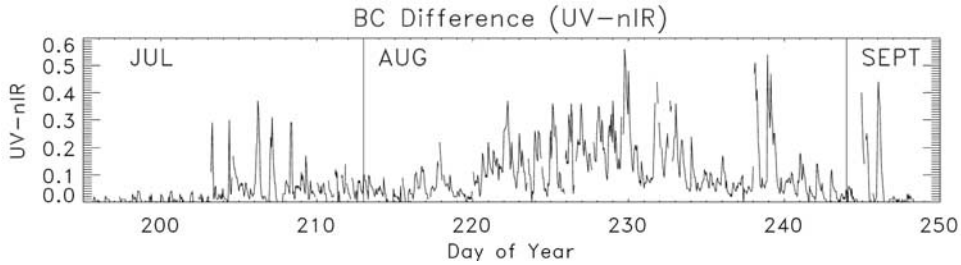

Figure 13. Timeline of the difference in the UV (λ = 370 nm) and near IR (nIR, λ = 880 nm) black carbon concentrations from a dual-wavelength aethalometer.

[33] The largest differences between the UV and nIR signals occurred during smoke events (see Figure 13). The wavelength dependence of absorption by biomass smoke aerosols, and tar balls in particular, is important because it suggests that these particles have spectral varying refractive indices resulting in more absorption than predicted by the usually assumed λ^{-1} dependence. Increases in the imaginary part of refractive index with decreasing wavelength has been shown to occur for flame soot [*Chang and Charalampopoulos*, 1990], and is also expected for highly conjugated systems presumed to exist in high–molecular weight HULIS. The wavelength dependence of absorption by tar balls (or other organic carbon particles) has important implications for remote sensing applications, climate forcing estimates [*Hatzianastassiou et al.*, 2004], and measurements of light-absorbing carbon that are typically performed at only one wavelength. The imaginary part of the complex refractive index of tar balls derived from EC data during YACS at 632 nm (k = 0.02) is consistent with spectrally varying estimates reported by *Kirchstetter et al.* [2004] for organic carbon from biomass burning aerosols (k = 0.017–0.005 for λ = 600–650 nm).

[34] The ESEM experiments of particle hygroscopicity indicate that tar balls observed during YACS are water soluble at high relative humidity (RH > 83%), albeit to a much lower degree than inorganic salt particles and with no distinct deliquescence point. The minimal growth of tar balls at high RH is consistent with other measurements during YACS that demonstrated only weak to no hygroscopic particle growth occurring during periods dominated by tar balls and other organic carbon aerosol types [*Carrico et al.*, 2005; *Day and Malm*, 2003; *Malm et al.*, 2005b]. Other reports of water-soluble refractory high–molecular weight carbon compounds in biomass smoke [*Novakov and Corrigan*, 1996; *Graham et al.*, 2002; *Mayol-Bracero et al.*, 2002] are consistent with our observations that tar balls are soluble at relative humidities that approach saturation. However, our ESEM experiments reveal that although tar balls are water-soluble, they are only weakly hygroscopic and changes in their size distributions or optical properties from hygroscopic growth would not be expected to occur for RH < 83%. However, the implications for the solubility of tar balls in the atmosphere are important. Tar balls possibly could be entrained inside existing liquid cloud droplets leading to their removal by wet scavenging. Also, tar balls may also serve as cloud condensation nuclei (CCN) at atmospherically relevant supersaturations, suggesting that they may play an important role in cloud formation and subsequent climate forcing effects.

5. Summary

[35] Analyses of individual particles using methods of electron microscopy revealed the presence of aged tar ball particles that were associated with long-range transport of biomass smoke to Yosemite National Park. The aging of the tar balls was revealed by electron energy loss maps that showed enhanced oxygen concentrations in the ~30 nm outer layer of the particle. Although tar balls have been observed previously during biomass smoke events, their ensemble average physical and optical properties and single particle hygroscopic properties have not been estimated. One of the unique contributions of this work to the understanding of tar ball properties is the concurrent measurements of aerosol composition, physical and optical properties and the ability to relate the presence of tar balls to these data. The presence of tar balls did not signal any detectable differences in aerosol density or derived aerosol refractive indices or require different assumptions compared to other types of organic aerosol particles to obtain closure in measured and reconstructed fine mass and light scattering coefficients. However, tar balls were associated with high ensemble average mass scattering efficiencies (~6 m^2 g^{-1}) because of their size distribution characteristics. Measurements of the hygroscopic properties of individual tar balls with ESEM indicate that tar balls do not exhibit deliquescence but are soluble at high (~83%) relative humidity. Although additional techniques may provide further distinctions between tar balls and other types of organic carbon particles (i.e., methods that can distinguish high–molecular weight compounds), compositional differences between tar balls and other types of organic particles were not distinguishable from CCSEM/EDX data. Tar ball morphological characteristics as defined by visual inspection of SEM images were distinct from other types of organic carbon particles, however this distinctiveness was not borne out in their ensemble average properties derived from other collocated aerosol measurements.

[36] The refractory and nongraphitic nature of tar balls (as seen in the SEM and TEM) and the absence of soot from SEM samples suggest that during the YACS study organic and elemental carbon, as characterized by thermal optical reflectance (TOR), should not be interpreted as an external mixture of organic and elemental carbon, but rather as nongraphitic carbonaceous particles containing light absorbing molecules (e.g., tar balls). The ability of tar balls to absorb light is further supported by their association with high concentrations of light absorbing carbon as derived from a dual wavelength aethalometer.

[37] The derived ensemble average optical properties of tar balls suggest they could play an important role in regional haze and climate forcing because they are especially efficient at scattering light and they exhibit wavelength-dependent light absorption properties. Although they exhibit only minimal growth at high RH, they could serve as cloud condensation nuclei (CCN) at atmospherically relevant supersaturations.

[38] **Acknowledgments.** The National Park Service funded YACS. Air Resource Specialists are gratefully acknowledged for their assistance, and Russell Galipeau, Katy Warner, and the resource managers at Yosemite National Park were helpful in the logistics of the sampling site. Electron microscopy analyses were performed in the Environmental Molecular Sciences Laboratory (EMSL), a national scientific user facility sponsored by the Department of Energy's Office of Biological and Environmental Research at Pacific Northwest National Laboratory (PNNL). PNNL is operated by the U.S. Department of Energy by Battelle Memorial Institute under contract DE-AC06-76RL0 1830. The PNNL research group acknowledges support provided from Laboratory Directed Research and Development funds of PNNL and the Atmospheric Science Program of the Office of Biological and Environmental Research (OBER), U.S. Department of Energy. Authors also thank two anonymous reviewers for their thorough evaluation of this manuscript. Their detailed and helpful suggestions improved the quality of this manuscript.

References

Alfaro, S. C., A. Gaudichet, J. L. Rajot, L. Gomes, M. Maillé, and H. Cachier (2003), Variability of aerosol size-resolved composition

at an Indian coastal site during the Indian Ocean Experiment (INDOEX) intensive field phase, *J. Geophys. Res.*, *108*(D8), 4235, doi:10.1029/2002JD002645.

Allen, G. A., P. Babich, and R. L. Poirot (2004), Evaluation of a new approach for real time assessment of wood smoke PM, paper presented at Visibility Specialty Conference on Regional and Global Perspectives on Haze: Causes, Consequences and Controversies, Air Waste Manage. Assoc., Asheville, N. C., 25–29 Oct.

Armstrong, J. T. (1991), Quantitative elemental analysis of individual microparticles with electron beam instruments, in Electron Probe Quantitation, edited by K. F. J. Heinrich and D. E. Newbury, pp. 261–316, Springer, New York.

Bergstrom, R. W., P. B. Russell, and P. Hignett (2002), Wavelength dependence of the absorption of black carbon particles: Predictions and results from the TARFOX experiment and implications for the aerosol single scattering albedo, *J. Atmos. Sci.*, *59*, 567–577.

Bohren, C. F., and D. R. Huffman (1983), *Absorption and Scattering of Light by Small Particles*, Wiley-Interscience, Hoboken, N. J.

Bond, T. C., D. G. Streets, K. F. Yarber, S. M. Nelson, J.-H. Woo, and Z. Klimont (2004), A technology-based global inventory of black and organic carbon emissions from combustion, *J. Geophys. Res.*, *109*, D14203, doi:10.1029/2003JD003697.

Carrico, C. M., S. M. Kreidenweis, D. Day, J. Collett Jr., T. Lee, J. Carrillo, G. R. McMeeking, and W. C. Malm (2005), Hygroscopic growth behavior of a carbon dominated aerosol inYosemite National Park, *Atmos. Environ.*, *39*, 1393–1404.

Chang, H., and T. T. Charalampopoulos (1990), Determination of the wavelength dependence of refractive indices of flame soot, *Proc. R. Soc. London, Ser. A*, *430*, 577–591.

Chow, J. C., J. G. Watson, L. C. Pritchett, W. R. Pierson, C. A. Frazier, and R. G. Purcell (1993), The DRI thermal/optical reflectance carbon analysis system: Description, evaluation and applications in U.S. air quality studies, *Atmos. Environ., Part A*, *27*(8), 1185–1201.

Cofer, W. R., III, J. S. Levine, D. I. Sebacher, E. L. Winstead, P. J. Riggen, J. A. Brass, and V. G. Ambrosia (1988), Particulate emissions from a mid-latitude prescribed chaparral fire, *J. Geophys. Res.*, *93*(D5), 5207–5212.

Danilatos, G. D. (1993), Introduction to the ESEM instrument, *Microsc. Res. Tech.*, *25*(5–6), 354–361.

Day, D., and W. C. Malm (2003), Aerosol light scattering measurements as a function of relative humidity at Yosemite National Park, 96th Annual Conference, Air and Waste Manage. Assoc., San Diego, Calif., 22–26 June.

Ebert, M., S. Weinbruch, A. Rausch, G. Gorzawski, P. Hoffman, H. Wex, and G. Helas (2002), Complex refractive index of aerosols during LACE 98 as derived from the analysis of individual particles, *J. Geophys. Res.*, *107*(D21), 8121, doi:10.1029/2000JD000195.

Foot, J. S., and C. G. Kilsby (1989), Absorption of light by aerosol particles: An intercomparison of techniques and spectral observations, *Atmos. Environ.*, *23*(2), 489–495.

Formenti, P., W. Elbert, W. Maenhaut, J. Haywood, S. Osborne, and M. O. Andreae (2003), Inorganic and carbonaceous aerosols during the South African Regional Science Initiative (SAFARI 2000) experiment: Chemical characteristics, physical properties, and emission data for smoke from African biomass burning, *J. Geophys. Res.*, *108*(D13), 8488, doi:10.1029/2002JD002408.

Gaudichet, A., F. Echalar, B. Chatenet, J. P. Quisefit, G. Malingre, H. Cachier, P. Buat-Menard, P. Artaxo, and W. Maenhaut (1995), Trace elements in tropical African savanna biomass burning aerosols, *J. Atmos. Chem.*, *22*, 19–39.

Gelencsér, A., A. Hoffer, A. Molnár, Z. Krivácsy, G. Kiss, and E. Mészáros (2000), Thermal behaviour of carbonaceous aerosol from a continental background site, *Atmos. Environ.*, *34*, 823–831.

Gelencsér, A., A. Hoffer, G. Kiss, E. Tombácz, R. Kurdi, and L. Bencze (2003), In-situ formation of light absorbing organic matter in cloud water, *J. Atmos. Chem.*, *45*, 25–33.

Godoi, R. H. M., A. F. L. Godoi, A. Worobiec, S. J. Andrade, J. de Hoog, M. R. Santiago-Silva, and R. Van Grieken (2004), Characterisation of sugar cane combustion particles in the Araraquara region, Southeast Brazil, *Microchim. Acta*, *145*(1–4), 53–56.

Graham, B., O. L. Mayol-Bracero, P. Guyon, G. C. Roberts, S. Decesari, M. C. Facchini, P. Artaxo, W. Maenhaut, P. Köll, and M. O. Andreae (2002), Water-soluble organic compounds in biomass burning aerosols over Amazonia: 1. Characterization by NMR and GC-MS, *J. Geophys. Res.*, *107*(D20), 8047, doi:10.1029/2001JD000336.

Guyon, P., B. Graham, G. C. Roberts, O. L. Mayol-Bracero, W. Maenhaut, P. Artaxo, and M. O. Andreae (2003), In-canopy gradients, composition, sources, and optical properties of aerosol over the Amazon forest, *J. Geophys. Res.*, *108*(D18), 4591, doi:10.1029/2003JD003465.

Hasan, H., and T. G. Dzubay (1983), Apportioning light extinction coefficients to chemical species in atmospheric aerosol, *Atmos. Environ.*, *17*(8), 1573–1581.

Hatzianastassiou, N., B. Katsoulis, and I. Vardavas (2004), Sensitivity analysis of aerosol direct radiative forcing in ultraviolet-visible wavelengths and consequences for the heat budget, *Tellus, Ser. B*, *56*, 368–381.

Hoffer, A., G. Kiss, M. Blazsó, and A. Gelencsér (2004), Chemical characterization of humic-like substances (HULIS) formed from a lignin-type precursor in model cloud water, *Geophys. Res. Lett.*, *31*, L06115, doi:10.1029/2003GL018962.

Hoffman, R. C., A. Laskin, and B. J. Finlayson-Pitts (2004), Sodium nitrate particles: Physical and chemical properties during hydration and dehydration, and implications for aged sea salt aerosols, *J. Aerosol Sci.*, *35*(7), 869–887.

Hua, Y. N. (2003), Studies on quantification analysis of thin film layers (Si3N4, SiO2, and TiW) in wafer fabrication using energy-dispersive X-ray microanalysis technique and SEC factors, *J. Trace Microprobe Tech.*, *21*(1), 25–34.

Ishiguro, T., Y. Takatori, and K. Akihama (1997), Microstructure of soot particles probed by electron microscopy: First observation of inner core and outer shell, *Combust. Flame*, *108*, 231–234.

Kirchstetter, T. W., T. Novakov, and P. V. Hobbs (2004), Evidence that the spectral dependence of light absorption by aerosols is affected by organic carbon, *J. Geophys. Res.*, *109*, D21208, doi:10.1029/2004JD004999.

Laskin, A., and J. P. Cowin (2001), Automated single particle SEM/EDX analysis of submicrometer particles down to 0.1 μm, *Anal. Chem.*, *73*, 1023–1029.

Laskin, A., M. J. Iedema, and J. P. Cowin (2002), Quantitative time-resolved monitoring of nitrate formation in sea salt particles using an automated SEM/EDX single particle analysis, *Environ. Sci. Technol.*, *36*, 4948–4955.

Laskin, A., M. J. Iedema, and J. P. Cowin (2003), Time-resolved aerosol collector for CCSEM/EDX single-particle analysis, *Aerosol Sci. Technol.*, *37*, 246–260.

Laskin, A., J. P. Cowin, and M. J. Iedema (2005a), Off-line analysis of individual environmental particles using modern methods of electron microscopy and X-ray microanalysis, *J. Electron Spectrosc. Related Phenomena*, in press.

Laskin, A., M. J. Iedema, A. Ichkovich, E. R. Graber, I. Taraniuk, and Y. Rudich (2005b), Direct observation of completely processed calcium carbonate dust particles, *Faraday Discuss.*, *130*, 453–468.

Lee, T., C. Carrico, J. Carrillo, P. Herckes, G. Engling, S. M. Kreidenweis, and J. Collett Jr. (2003), Continuous measurement of aerosol ionic composition during the Yosemite National Park Special Study in 2002, paper presented at 96th Annual Conference, Air and Waste Manage. Assoc., San Diego, Calif., 22–26 June.

Li, J., M. Pósfai, P. V. Hobbs, and P. R. Buseck (2003a), Individual aerosol particles from biomass burning in southern Africa: 2. Compositions and aging of inorganic particles, *J. Geophys. Res.*, *108*(D13), 8484, doi:10.1029/2002JD002310.

Li, J., J. R. Anderson, and P. R. Buseck (2003b), TEM study of aerosol particles from clean and polluted marine boundary layers over the North Atlantic, *J. Geophys. Res.*, *108*(D6), 4189, doi:10.1029/2002JD002106.

Malm, W. C., J. F. Sisler, D. Huffman, R. A. Eldred, and T. A. Cahill (1994), Spatial and seasonal trends in particle concentration and optical extinction in the United States, *J. Geophys. Res.*, *99*(D1), 1347–1370.

Malm, W. C., D. E. Day, C. Carrico, S. M. Kreidenweis, J. L. Collett Jr., G. McMeeking, T. Lee, and J. Carrillo (2005a), Intercomparison and closure calculations using measurements of aerosol species and optical properties during the Yosemite Aerosol Characterization Study, *J. Geophys. Res.*, *110*, D14302, doi:10.1029/2004JD005494.

Malm, W. C., D. E. Day, S. M. Kreidenweis, J. L. Collett Jr., C. Carrico, G. McMeeking, and T. Lee (2005b), Hygroscopic properties of organic-laden aerosol, *Atmos. Environ.*, *39*, 4969–4982.

Maria, S. F., L. M. Russell, M. K. Gilles, and S. C. B. Myneni (2004), Organic aerosol growth mechanisms and their climate-forcing implications, *Science*, *306*, 1921–1924.

Martins, J. V., P. Artaxo, P. V. Hobbs, C. Liousse, H. Cachier, Y. Kaufman, and A. P. Fattori (1996), Particle size distributions, elemental compositions, carbon measurements, and optical properties of smoke from biomass burning in the Pacific Northwest of the United States, in *Biomass Burning and Global Change*, vol. 2, edited by J. Levine, pp. 716–732, MIT Press, Cambridge, Mass.

Martins, J. V., P. Artaxo, C. Liousse, J. S. Reid, P. V. Hobbs, and Y. J. Kaufman (1998), Effects of black carbon content, particle size, and mixing on light absorption by aerosols from biomass burning in Brazil, *J. Geophys. Res.*, *103*(D4), 32,041–32,050.

Mayol-Bracero, O. L., P. Guyon, B. Graham, G. Roberts, M. O. Andreae, S. Desesari, M. C. Facchini, S. Fuzzi, and P. Artaxo (2002), Water-soluble organic compounds in biomass burning aerosols over Amazonia:

2. Apportionment of the chemical composition and importance of the polyacidic fraction, *J. Geophys. Res.*, *107*(D20), 8091, doi:10.1029/2001JD000522.

McMeeking, G. R. (2004), Size distribution measurements of wildfire smoke-influenced aerosol at Yosemite National Park, M.S. thesis, Colo. State Univ., Fort Collins.

McMeeking, G. R., S. M. Kreidenweis, C. Carrico, T. H. Lee, J. L. Collett, and W. C. Malm (2005a), Observations of smoke-influenced aerosol during the Yosemite Aerosol Characterization Study: Size distributions and chemical composition, *J. Geophys. Res.*, *110*, D09206, doi:10.1029/2004JD005389.

McMeeking, G. R., S. M. Kreidenweis, C. Carrico, J. L. Collett, D. E. Day, and W. C. Malm (2005b), Observations of smoke-influenced aerosol during the Yosemite Aerosol Characterization Study: 2. Aerosol scattering and absorbing properties, *J. Geophys. Res.*, *110*, D18209, doi:10.1029/2004JD005624.

Mukai, H., and Y. Ambe (1986), Characterization of a humic acid-like brown substance in airborne particulate matter and tentative identification of its origin, *Atmos. Environ.*, *20*(5), 813–819.

Novakov, T., and C. E. Corrigan (1995), Thermal characterization of biomass smoke particles, *Mikrochim. Acta*, *119*, 157–166.

Novakov, T., and C. E. Corrigan (1996), Cloud condensation nucleus activity of the organic component of biomass smoke particles, *Geophys. Res. Lett.*, *23*(16), 2141–2144.

Osán, J., B. Alföldy, S. Török, and R. Van Grieken (2002), Characterization of wood combustion particles using electron probe microanalysis, *Atmos. Environ.*, *36*, 2207–2214.

Ouimette, J. R., and R. C. Flagan (1982), The extinction coefficient of multicomponent aerosols, *Atmos. Environ.*, *16*(10), 2405–2419.

Patterson, E. M., and C. K. McMahon (1984), Absorption characteristics of forest fire particulate matter, *Atmos. Environ.*, *18*(11), 2541–2551.

Pósfai, M., R. Simonics, J. Li, P. V. Hobbs, and P. R. Buseck (2003), Individual aerosol particles from biomass burning in southern Africa: 1. Compositions and size distributions of carbonaceous particles, *J. Geophys. Res.*, *108*(D13), 8483, doi:10.1029/2002JD002291.

Pósfai, M., A. Gelencser, R. Simonics, K. Arato, J. Li, P. V. Hobbs, and P. R. Buseck (2004), Atmospheric tar balls: Particles from biomass and biofuel burning, *J. Geophys. Res.*, *109*, D06213, doi:10.1029/2003JD004169.

Rogge, W. F., L. M. Hildemann, M. A. Mazurek, G. R. Cass, and B. R. T. Simoneit (1998), Sources of fine organic aerosol: 9. Pine, oak, and synthetic log combustion in residential fireplaces, *Environ. Sci. Technol.*, *32*, 13–22.

Rupprecht, G., H. Patashnick, D. E. Beeson, R. N. Green, and M. B. Meyer (1995), A new automated monitor for the measurement of particulate carbon in the atmosphere, paper presented at Conference on Particulate Matter: Health and Regulatory Issues, Air and Waste Manage. Assoc., Pittsburgh, Pa.

Turpin, B. J., and H.-J. Lim (2001), Species contributions to PM2.5 mass concentrations: Revisiting common assumptions for estimating organic mass, *Aerosol Sci. Technol.*, *35*, 602–610.

Yuan, H., K. A. Rahn, and G. Zhuang (2004), Graphical techniques for interpreting the composition of individual aerosol particles, *Atmos. Environ.*, *38*, 6845–6854.

Zuberi, B., K. S. Johnson, G. K. Aleks, L. T. Molina, M. J. Molina, and A. Laskin (2005), Hydrophilic properties of aged soot, *Geophys. Res. Lett.*, *32*, L01807, doi:10.1029/2004GL021496.

C. Carrico, J. Carrillo, J. Collett Jr., and T. Lee, Department of Atmospheric Science, Colorado State University, Fort Collins, CO 80523, USA.

J. P. Cowin, Chemical Sciences Division, Pacific Northwest National Laboratory, P.O. Box 999, K8-88, Richland, WA 99352, USA.

D. Day and J. L. Hand, Cooperative Institute for Research in the Atmosphere, Colorado State University, Fort Collins, CO 80523, USA. (hand@cira.colostate.edu)

M. J. Iedema, A. Laskin, and C. Wang, William R. Wiley Environmental Molecular Sciences Laboratory, Pacific Northwest National Laboratory, P.O. Box 999, MSIN: K8-88, Richland, WA 99352, USA. (alexander.laskin@pnl.gov)

W. C. Malm, National Park Service, Cooperative Institute for Research in the Atmosphere, Colorado State University, Fort Collins, CO 80523, USA.